Cancer Immunology, Immunotherapy (2019) 68:257–268
https://doi.org/10.1007/s00262-018-2270-5

ORIGINAL ARTICLE

Hyperresponsiveness to interferon gamma exposure as a response mechanism to anti-PD-1 therapy in microsatellite instability colorectal cancer

Wenli Yuan[1] · Deyao Deng[1] · Hongchao Jiang[3] · Changling Tu[4] · Xueqin Shang[5] · Hongchun He[6] · Ruize Niu[7] · Jian Dong[2]

Received: 16 January 2018 / Accepted: 31 October 2018 / Published online: 7 November 2018

Abstract

Colorectal cancer (CRC) with high-level microsatellite instability (MSI-H) tends to be associated with a better response to programmed death receptor-1 (PD-1) blockade than does microsatellite stable CRC. However, emerging evidence makes the use of programmed death ligand-1 (PD-L1) as a biomarker problematic. Here, we sought to characterize the interactions between PD-L1 expression and the response to PD-1 blockade therapy in BALB/c mice with a subcutaneous tumor challenge. We further focused on interferon gamma (IFNγ)-induced PD-L1 expression in an in vitro setting to evaluate the responsiveness to IFNγ exposure and the specific signaling of PD-1 in HCT116 and SW480 cell lines. In this study, enhanced PD-L1 expression increased survival in CT26 cells, and PD-1 blockade increased the CTL profile and apoptotic cells in mice with CRC. Our in vitro findings showed that PD-L1 expression was significantly upregulated by a low-dose IFNγ treatment, and the MSI-H cell line might exhibit hyperresponsiveness to IFNγ exposure partly through the JAK–STAT pathway. These results suggest that intrinsic PD-L1 in cooperation with extrinsic IFNγ exposure in CRC may be more responsive to anti-PD-1 therapy, mainly through the CTL profile in the tumor microenvironment.

Keywords Colorectal cancer · Microsatellite instability · IFNγ · PD-L1 · CTL

Abbreviations

CRC	Colorectal cancer
CTL	Cytotoxic T lymphocyte
DAPI	4′,6-Diamidino-2-phenylindole
EGFR	Epidermal growth factor receptor
FCM	Flow cytometry
HE	Hematoxylin and eosin
IFNγ	Interferon gamma

Electronic supplementary material The online version of this article (https://doi.org/10.1007/s00262-018-2270-5) contains supplementary material, which is available to authorized users.

✉ Jian Dong
jiandong20140901@yeah.net

[1] Department of Clinical Laboratory, The Fourth Affiliated Hospital of Kunming Medical University, Kunming 650021, People's Republic of China

[2] The Third Affiliated Hospital of Kunming Medical University, Yunnan Cancer Hospital, Yunnan Cancer Center, No. 519 Kun Zhou Road, Xishan District, Kunming 650118, Yunnan, People's Republic of China

[3] The Affiliated Children's Hospital of Kunming Medical University, Kunming 650228, People's Republic of China

[4] Department of Cadre Medical Branch, Yunnan Cancer Hospital, Yunnan Cancer Center, The Third Affiliated Hospital of Kunming Medical University, Kunming 650118, People's Republic of China

[5] Department of Oncology, The Fourth Affiliated Hospital of Kunming Medical University, Kunming 650021, People's Republic of China

[6] Department of General Surgery, The Fourth Affiliated Hospital of Kunming Medical University, Kunming 650021, People's Republic of China

[7] Department of Laboratory Zoology, Kunming Medical University, Kunming 650500, People's Republic of China

JAK/STAT3	Janus kinase/signal transducer and activator of transcription 3
MAPK	Mitogen-activated protein kinase
MSI-H	High-level microsatellite instability
MSS	Microsatellite stable
PD-1	Programmed death-1
PD-L1	Programmed death ligand-1
PI3K/AKT	Phosphatidylinositol 3 kinase/protein kinase B
PTEN	Phosphatase and tensin homology deleted on chromosome 10
RT-PCR	Reverse-transcription quantitative polymerase chain reactions
TUNEL	TdT-mediated dUTP nick-end labeling

Introduction

Colorectal cancer (CRC) is one of the most common cancers worldwide and is often considered immunogenic, especially high-level microsatellite unstable (MSI-H) CRC [1]. This perception is based on the observation that MSI-H CRCs have a high burden of neoantigens with collinearity of intratumoral lymphocytic infiltration [2, 3]. A characteristic of this type of cancer is its ability to escape detection and destruction by the immune system through genetic or epigenetic modifications. This ability mainly involves the production of immunosuppressive cytokines [4] and enzymes [5], favoring conversion of immune effector cells into immunosuppressive cell populations [6] or upregulation of the tumor cell surface inhibitory B7 costimulatory molecule programmed death ligand 1 (PD-L1) [7]. After binding to its receptor, programmed death receptor-1 (PD-1), PD-L1 delivers a suppressive signal to T cells and an anti-apoptotic signal to tumor cells, leading to T cell dysfunction and tumor survival. Blockade of PD-1/PD-L1 results in the preferential activation of T cells with specificity for cancer, restoring anti-tumor T cell activity [8–10]. In particular, inhibitors of the PD-1/PD-L1 pathway have led to remarkable clinical responses in melanoma [8], non-small-cell lung cancer [9], and renal cancer [10].

PD-1 inhibition is an exciting new frontier and was recently approved by the US FDA for adults with MSI-H progressive CRC; however, the response to PD-1 blockade is uniform across all MSI-H CRC patients. In general, the limited data [2, 11, 12] from available clinical trials show that patients with MSI-H CRC have more objective responses to PD-1 blockade than do patients with microsatellite stable (MSS) tumors. This finding leads to the question of what is different between these two subgroups. Recent manuscripts [2, 11, 12] have demonstrated that compared with patients with MSS tumors, patients with MSI-H tumors have increased expression of PD-L1 accompanied by a linear increase in the infiltration density of activated $CD8^+$ cytotoxic T lymphocytes (CTLs). Although there is a substantial difference in PD-L1 expression between MSI-H and MSS CRCs, the general evidence for PD-L1 expression as a responsive mechanism to anti-PD-1 therapy in CRC is less clear. PD-L1 is induced by IFNγ treatment of cancer cells [14]. Therefore, IFNγ signaling appears to participate in the vigorous immune microenvironment of MSI-H CRC.

IFNγ induces anti-tumor responses with cytostatic, pro-apoptotic and immune-provoking effects [15]. Nevertheless, cancer cells can also take advantage of the same IFNγ signaling processes as inducers of mediators that inhibit anti-tumor immune reactions, such as PD-L1 [15, 16]. PD-L1 is expressed at various levels in cultured cancer cell lines, and the different expression levels may be associated with intrinsic cellular changes, such as Janus kinase-signal transducer and activator of transcription 3 (JAK-STAT3) and phosphatidylinositol 3 kinase–protein kinase B (PI3K–AKT) activation [17], loss/deficiency of phosphatase and tensin homology deleted on chromosome (PTEN) [18], and epidermal growth factor receptor (EGFR) mutations [19]. Tumor-infiltrating lymphocytes produce IFNγ, which drives PD-L1 expression in the tumor microenvironment; however, the extent of PD-L1 induction is not uniform [14–16]. The rate of $PD\text{-}L1^+$ expression is significantly higher in MSI-H CRC than in MSS CRC [2, 11, 12, 13, 20]. Recent findings [11, 21] also note that PD-L1 expression in tumor tissue probably indicates possible biomarkers to predict which patients will most likely benefit from anti-PD-1 therapy, particularly among those with MSI-H CRC. This intratumoral immune response induced by IFNγ signaling appears to be more effective in MSI-H tumors, and the distinct molecular mechanisms of this type of extrinsic IFNγ induction in MSI-H and MSS CRCs may exist. In this regard, clarifying this paradoxical mechanistic basis is significant.

In the current study, we investigated whether elevated expression of PD-L1 in tumor tissues had a more objective response to PD-1 blockade in BALB/c mice with subcutaneous tumors. The average extent of inflammation and adaptive immunity factors as well as cellular apoptosis in the specific tumor microenvironment was also investigated. Distinct molecular mechanisms of IFNγ have been proposed to induce PD-L1 expression in MSI-H and MSS CRC cell lines. To test this hypothesis, we used HCT116 and SW480 cells in vitro to observe the signaling mechanism of the adaptive immunity response induced by IFNγ.

Materials and methods

Cell lines and cultures

HCT116, SW480 and CT26 cell lines were routinely cultured in DMEM/F12 (Gibco, USA) and supplemented with

10% fetal bovine serum (Gibco, USA), 100 IU/mL penicillin and 100 μg/mL streptomycin (Gibco, USA) at 37 °C in 5% CO_2.

Generation of a stable PD-L1-overexpressing CT26 cell line

The cDNA sequence of the mouse PD-L1 was generated by PCR using 5′-CCGGAATTC GCCACCATGAGGATA TTTGCTGGCATTATATTC-3′ as the forward primer and 5′-CCGCTCGAG TTACGTCTCCTCGAATTGTGTATC A-3′ as the reverse primer. The plasmid was sequenced with the primers to confirm the correctness of the constructed plasmid. Lentiviruses were produced by transient transfection of 293T cells using PGMLV-GTP-PD-L1. After transfection, virus samples were harvested at 72 h and concentrated. The virus titer was measured. Transduction of CT26 cells was performed by 6 h of exposure to dilutions of the viral supernatant in the presence of polybrene (5 μg/mL). Stably transfected CT26 cells were selected by culture in puromycin (2 μg/mL).

Tumor challenge and antibody treatment

The experiments were conducted on female BALB/c mice weighing 16–20 g. For tumor generation, the animals were challenged subcutaneously in the right flank with 5×10^7 CT26 in 100 μL PBS (group 1, 2, 5, and 6) or 5×10^7 PD-L1-overexpressing CT26 cells in 100 μL PBS (group 3 and 4). When the tumor volume reached approximately 80 mm^3 (on day 15 after injection), the animal model was successfully established. Furthermore, CRC mice were divided into six groups (six mice per group) treated with PD-1 monoclonal antibody (PD-1 mAb, Bio X Cell), IFNγ exposure combined with PD-1 mAb, or saline. Group 1 and group 3 were treated with saline, and group 5 was treated with IFNγ and saline. Group 2 represented mice treated with CT26 cells and PD-1 mAb; group 4 included mice treated with PD-L1-overexpressing CT26 cells plus PD-1 mAb; group 6 included mice treated with CT26 cells plus IFNγ and PD-1 mAb. PD-1 mAb (200 μg) was injected peritumorally into mice on days 0, 2, 4, 6 and 8 after successful tumor establishment, and IFNγ (100 IU/mL) was administered 2 days before PD-1 treatment. Following tumor establishment, tumors were monitored every 3 days. Tumor volume was calculated according to the following formula: volume = (the maximum diameter) × (the most trials)^2 × 0.5 [22]. Mice were sacrificed on day 30, and tumors were harvested, weighed and divided into parts for PCR analysis, western blot analysis, histological analysis and TdT-mediated dUTP nick-end labeling (TUNEL).

RT-PCR

Total cell RNA was extracted using TRIzol reagent (Thermo, USA) according to the manufacturer's protocol. RNA was then reverse transcribed with a Revert First Strand cDNA Synthesis Kit (Thermo, USA) according to the manufacturer's instructions. Reverse-transcription quantitative polymerase chain reaction (RT-PCR) was performed using an ABI-7500 (Applied Biosystems, USA). The primer sequences are shown in Supplementary Table 1.

IFNγ treatment in vitro and quantitative DNA array

To assess PCR array performance, we pretreated HCT116 and SW480 cells with 100 IU/mL IFNγ (PeproTech, USA) or control medium for 12 h, followed by washing and harvesting. A total RNA extraction kit was used to extract total RNA (Qiagen, Maryland, USA). Next, 0.5 μg total RNA was reverse transcribed. cDNA was mixed with RT^2 SYBR Green/ROX qPCR Master Mix (Qiagen, Maryland, USA), and the mixture was added to a 96-well RT^2 PCR Array (Qiagen, Maryland, USA) that contained primers for 84 genes associated with the JAK/STAT signal pathway and 5 housekeeping genes according to the manufacturer's instructions. Thermal cycling was performed using an ABI-7500. The cycle threshold (Ct) values obtained during quantification were used to calculate the fold changes in mRNA abundance using the $2^{-\Delta\Delta Ct}$ method.

Western blotting

Cells were harvested in RIPA lysis buffer (Bi Yun Tian, China) containing 50 μL protease inhibitor (Bi Yun Tian, China). The cell lysates (80 μg) were separated using 10% SDS–PAGE gels and then transferred onto PVDF membranes (Millipore, Bedford, MA, USA). Membranes were blocked with 5% bovine serum albumin for 1 h at room temperature before the addition of 5 mL primary antibody. The antibodies used in this study included anti-PD-L1 (1:500; Proteintech) and anti-GAPDH (1:2000; Abmart). The membrane was then washed with PBS and incubated with rabbit anti-HRP-conjugated secondary antibody (1:2000; Abmart) for 1 h at room temperature. Bands were visualized using a chemiluminescence reagent (Millipore, USA).

Flow cytometry

Cell samples were harvested, washed and stained with 5 μL anti-human CD274-PE (clone: MIH1, eBioscience) for 30 min; light exposure was avoided. Cells were washed, resuspended in 500 μL PBS and transferred to FACS tubes for analysis. Cells were analyzed using a Canto II (BD Biosciences) FACS machine. Data analysis was performed using

CellQuest Pro (BD Biosciences) and FlowJo software (Tree Star).

Hematoxylin and eosin (HE) staining and immunofluorescence costaining

Paraffin-fixed tissue samples were cut into sections of 5-μm thickness and stained with HE for histological examination. Immunofluorescence double staining was further performed to evaluate the histomorphological expression features of PD-L1. Sections were incubated with primary anti-PD-L1 (1:300; Proteintech) and anti-CD31 (1:150; Abcam)/anti-CD8 (1:100; Abcam) antibodies at 4 °C overnight. After the sections were washed with PBS, they were incubated with Cy3-labeled goat anti-rabbit IgG antibodies (red, 1:1000; KPL) and Dylight 488-labeled goat anti-mouse/rat IgG antibodies (green, 1:1000; Abcam) as the secondary antibodies. Finally, the sections were incubated with 4′,6-diamidino-2-phenylindole (DAPI) to stain the nuclei (blue color) and were observed by a fluorescence microscope (Olympus).

TUNEL assay and double staining for TUNEL and CD31

TUNEL staining was performed using an *in situ* cell death detection kit (Roche), and nuclei were stained with DAPI. For fluorescence double staining, sections were incubated with primary anti-CD31 (1:150; Abcam) for 1 h at 37 °C. After the sections were washed with PBS, they were incubated with the TUNEL reaction mixture plus Dylight 488 labeled goat anti-mouse IgG antibody (green, 1:1000; Abcam). The sections were washed, stained with DAPI, and observed by a fluorescence microscope.

Statistical analysis

All statistical analyses were performed using SPSS software version 22.0. Values are presented as the mean ± SDs, and the differences between groups were assessed with two-sided tests. Statistical significance was set at p values less than 0.05.

Results

Anti-tumor effects of PD-1 blockade

To investigate whether PD-L1 expression influences the response to PD-1 blockade immunotherapy in vivo, we examined two different profiles with higher PD-L1 expression in the subcutaneous tumor tissues of mice with CRC and PD-L1-transduced CT26 cell challenge with extrinsic IFNγ exposure. As shown in Fig. 1a, b, PD-L1 expression was higher in these two profiles and resulted in obviously enhanced subcutaneous tumor weights in CRC mice. Furthermore, immunotherapy with PD-1 blockade significantly inhibited tumor growth, especially in mice challenged with PD-L1-transduced CT26 cells (Fig. 1d). Mice treated with the combination of PD-1 blockade and IFNγ exposure (or PD-L1 transduction) had a slightly larger tumor weight on day 30; however, no significant difference was observed.

IFNγ exposure induced extensive PD-L1 expression, and PD-1 blockade caused decreased neoplastic cells

As shown in Fig. 2a, b, IFNγ treatment induced higher PD-L1 expression in the tumor tissues of BALB/c mice challenged with CT26 cells subcutaneously, accompanied by a decreased number of $CD8^+$ cells. To investigate whether higher PD-L1 expression was localized to tumor cells or tumor-infiltrating $CD8^+$ cells, we further performed fluorescence double staining for PD-L1 and CD31/CD8. Fluorescence costaining demonstrated that PD-L1 protein was extensively expressed on neoplastic cells as well as tumor-infiltrating $CD8^+$ lymphocytes (Fig. 2). However, low-level IFNγ exposure obviously enhanced the density of PD-L1 expression in both cell types in the tumor microenvironment. PD-1 blockade immunotherapy clearly decreased the number of CT26 neoplastic cells. However, a simultaneously increased number of $CD8^+$ lymphocytes were also observed, especially in IFNγ-treated mice (Fig. 2c).

PD-1 blockade induced obvious cell apoptosis

To determine the cell apoptosis rate in each group, we performed apoptotic analysis of tumor tissues by TUNEL. A decreased number of TUNEL-positive cells were detected in PD-L1-transduced CT26 cell-challenged animals. Treatment with PD-1 blockade significantly increased the rate of TUNEL-positive cells in all CRC mice; however, no significant difference was observed among CT26, PD-L1-transduced CT26 and IFNγ exposure plus CT26-injected animals (Fig. 3). To determine whether apoptosis involved neoplastic cells, we also used fluorescence double staining for TUNEL and CD31. As shown in Fig. 3, apoptotic neoplastic cells were observed in many groups, especially in CRC mice treated with PD-1 blockade. Importantly, more apoptotic CT26 cells existed in tumors harvested from CRC mice exposed to IFNγ combined with anti-PD-1 immunotherapy. However, the number of apoptotic neoplastic cells was lower in the other groups, and further statistical analysis was not performed in this experiment.

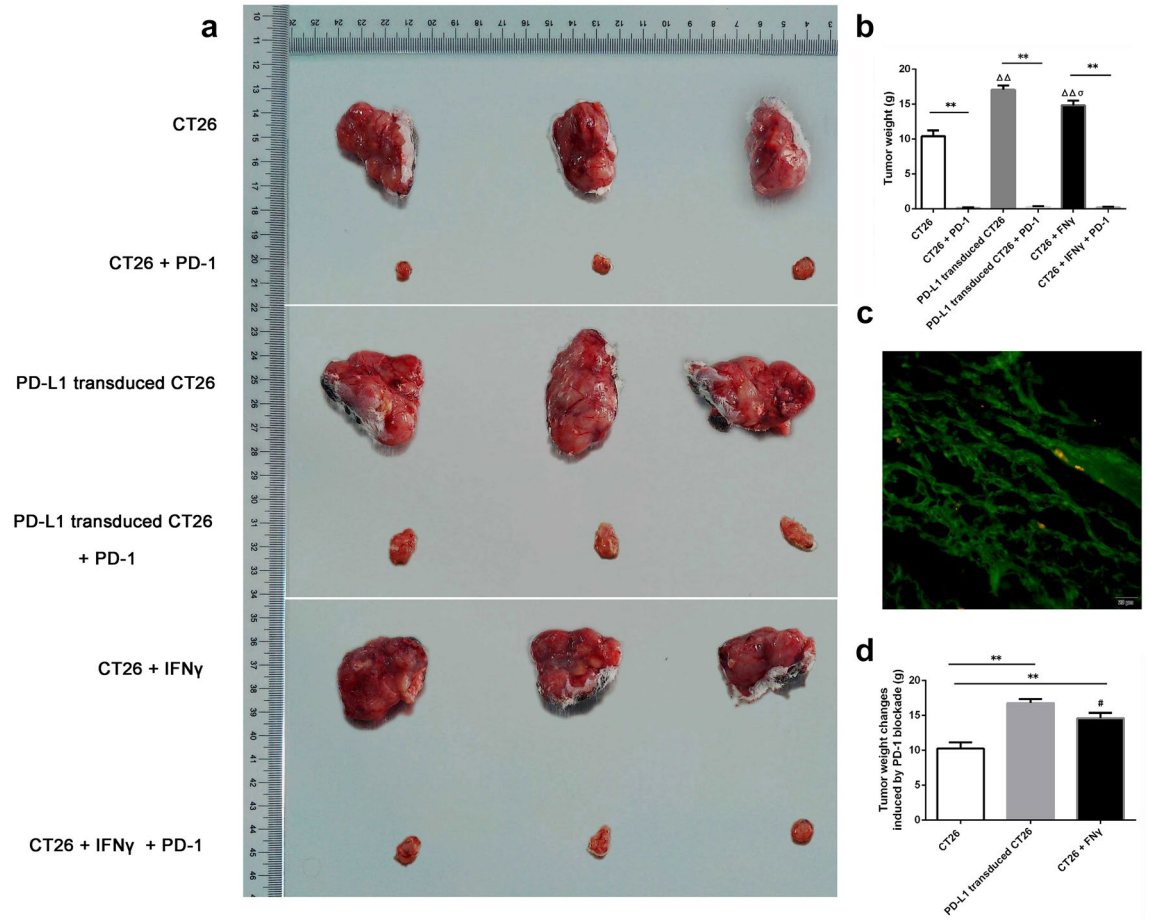

Fig. 1 Effects of PD-1 blockade in BALB/c mice with subcutaneous tumors in each group. When CRC animal models subcutaneously injected with CT26 cells (group 1, 2, 5, 6) or PD-L1-transduced CT26 cells (group 3, 4) were successfully established, they were divided into six groups treated with PD-1 blockade therapy with IFNγ plus PD-1 blockade or saline. PD-1 mAb (200 μg) was injected peritumorally on days 0, 2, 4, 6 and 8 after the successful establishment of animal models, and IFNγ (100 IU/mL) was administered 2 days before PD-1 immunotherapy. Those animal models were sacrificed, and tumors were harvested on day 30. **a** Tumor sizes of different groups; **b** statistics of the tumor weights in the six groups (**$p < 0.001$, $^{\Delta\Delta}p < 0.001$ vs. CT26, $^{\sigma}p < 0.05$ vs. PD-L1 transduced CT26); **c** photo showing PD-L1-overexpressing CT26 cells marked with green fluorescence protein as shown by fluorescence microscopy (×40, scale bar is 20 μm); **d** statistics of the tumor weight changes induced by PD-1 blockade in three different profiles (**$p < 0.001$, $^{\#}p < 0.05$ vs. PD-L1 transduced CT26)

PD-L1 overexpression influenced the adaptive immunity factors in response to PD-1 blockade

To observe the effect of PD-L1 overexpression on the average extent of adaptive immunity factors in response to anti-PD-1 immunotherapy, we performed RT-PCR for selected genes encoding signature T cell cytokines as well as core transcription factors for the major T helper subsets, CD4, Th1/Tc1 (TBX21 and IFNγ), CTL (CD8A, GZMB, PRF1, and IL21), Th17 (IL-17A, RORC, and IL23A) and Treg (FOXP3, IL10, and TGF-β1). Additionally, the sets of genes associated with immune checkpoints (CTLA-4 and LAG3) and metabolic enzymes (IDO1, NOS2, and HIF1A) were analyzed (Fig. 4a, b). In response to immunotherapy with PD-1 mAb, CD8a and GZMB were prominently enhanced, especially in tumors harvested from the PD-L1 transduced CT26 group. The expression of CD8a was clearly decreased when challenged with PD-L1 overexpression, whereas it was significantly increased in response to PD-1 mAb (Fig. 4c).

IFNγ induced a higher intensity of PD-L1 expression in HCT116 and SW480

In this experiment, we detected the expression of PD-L1 in HCT116 and SW480 cells induced by IFNγ via RT-PCR, western blot analysis and FCM. Treatment with different concentrations of IFNγ significantly increased PD-L1 expression

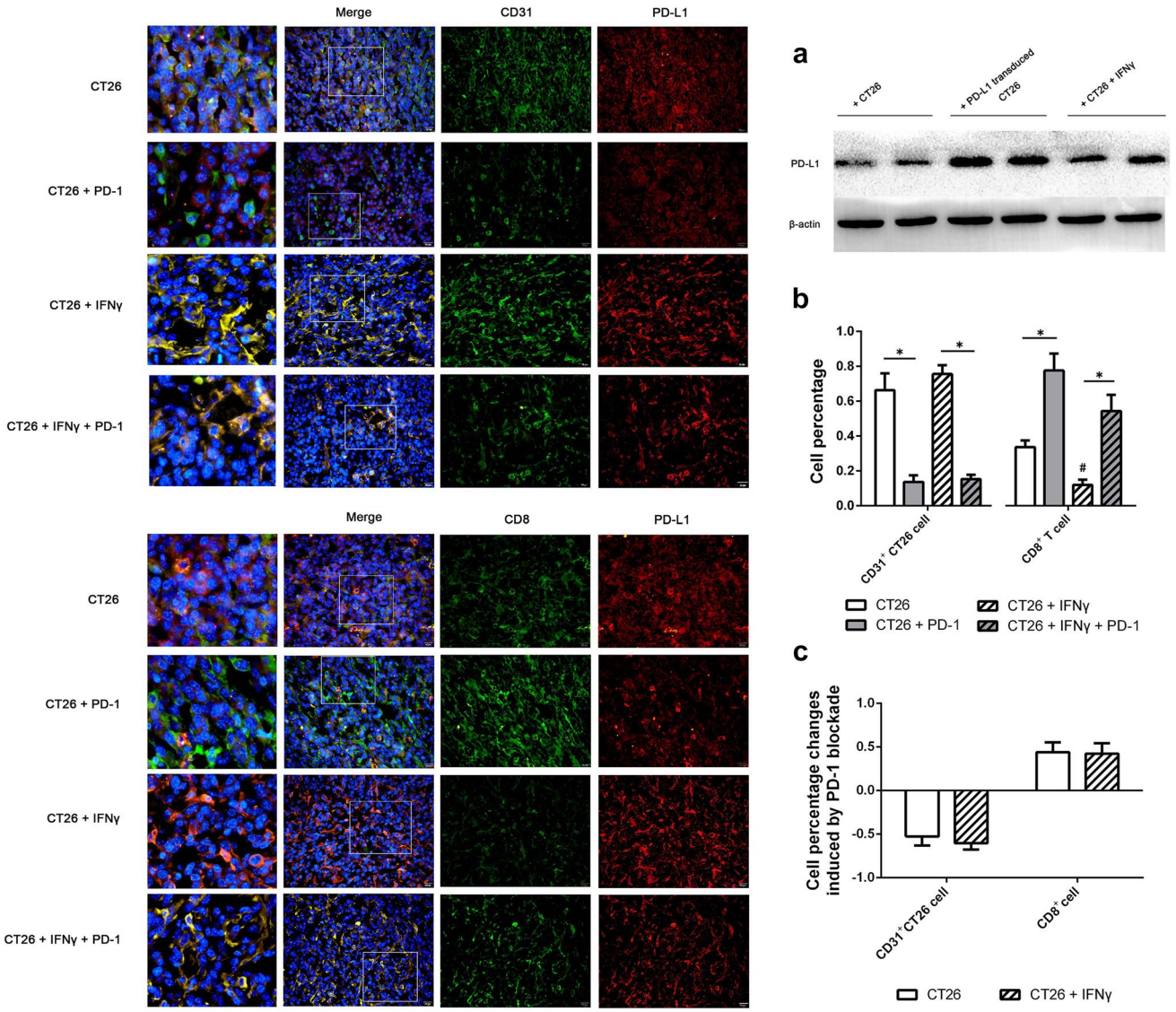

Fig. 2 Effects of IFNγ exposure combined with PD-1 blockade in tumor-infiltrated tissues. To investigate whether PD-L1 expression was localized to tumor cells or tumor-infiltrating $CD8^+$ cells, we performed fluorescence double staining for PD-L1 and CD31/CD8, respectively. The nucleus is shown in blue by DAPI. On the cell membrane, the PD-L1 marker is shown in red, and CD31/CD8 is green in a single stain. Merged staining is shown in yellow/orange on the membrane, and blue indicates the nucleus, which reveals PD-$L1^+CD31^+$ tumor cells or PD-$L1^+CD8^+$ lymphocytes, respectively. A magnified image of the area marked by the white square is shown in the leftmost column. Scale bars, 20 μm. **a** Expression of PD-L1 protein induced by PD-L1 transduced or IFNγ exposure in tumor-infiltrated tissues. **b** The cell percentage statistics of $CD31^+$ CT26 cells and $CD8^+$ lymphocytes in tumors harvested from group 1 and 2 and group 5 and 6 animal models ($^{**}p < 0.001$, $^{\#}p < 0.05$ vs. CT26). **c** Statistics of the cell percentage changes induced by PD-1 blockade with a focus on $CD31^+$ CT26 cells and $CD8^+$ lymphocytes

in HCT116 and SW480 cells in vitro, especially with 100 IU/mL IFNγ. Moreover, cultured SW480 and HCT116 cells became round and non-adherent after treatment with 5000 IU/mL IFNγ (data not shown). Interestingly, the PD-L1 expression observed in HCT116 cells induced by IFNγ was significantly higher than that induced by the same treatment in SW480 cells (Fig. 5).

Upregulation of PD-L1 by IFNγ in HCT116 and SW480 cells was mainly associated with JAK–STAT but not MAPK or PI3K–AKT pathway activation

To explore the signaling mechanism of PD-L1 expression induced by a low dose of IFNγ (100 IU/mL) in HCT116 and SW480 cells, we evaluated the expression of PD-L1

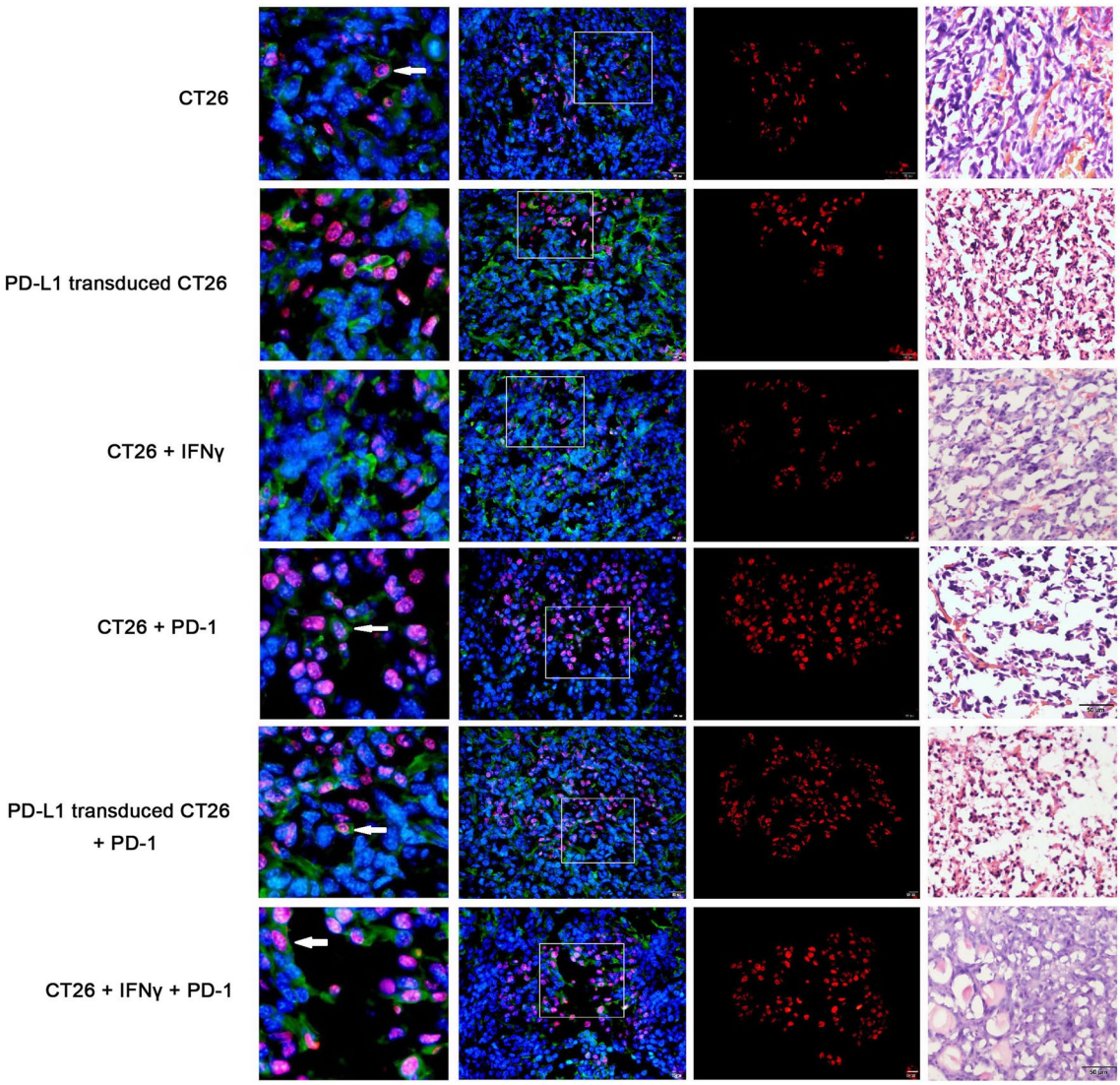

Fig. 3 PD-1 blockade induced cell apoptosis in BALB/c mice with subcutaneous tumors. Cell apoptosis shown by TUNEL-CD31 double staining (the left column, ×40, scale bar is 20 μm) and pathological changes shown by HE staining (the rightmost column, HE×200, scale bar is 50 μm) in the six groups. Shown by fluorescence microscopy, red indicates apoptotic cells stained by TUNEL, blue indicates nuclei stained by DAPI, and green indicates a CD31 marker in a single stain. Merged apoptotic cells are shown in pink in the nucleus. Apoptotic CT26 cells are shown with pink nuclei and green membranes. A magnified image of the area marked by the white square is shown in the leftmost column. The white arrow denotes apoptotic CT26 cells, which are shown in green in the membrane and pink in the nucleus. The number of TUNEL-positive cells (red color) and total number of cells (blue color) were captured with a fluorescence microscope. The rate of cell apoptosis was measured by the number of red cells divided by the number of blue cells. The apoptotic rate was (5.23 ± 0.91)% in group 1 (CT26), (3.47 ± 0.35)% in group 3 (PD-L1 transduced CT26), (4.13 ± 0.91)% in group 5 (CT26 + IFNγ), (30.67 ± 5.13)% in group 2 (CT26 + PD-1), (29.33 ± 4.04)% in group 4 (PD-L1-transduced CT26 + PD-1), and (24.33 ± 5.03)% in group 6 (CT26 + IFNγ + PD-1). The apoptosis rate of group 3 was significantly decreased compared with that of group 1 ($p = 0.042$). PD-1 blockade significantly induced an increased apoptosis rate in CT26-injected ($p = 0.018$), PD-L1-transduced CT26 cell-challenged ($p = 0.007$) or IFNγ-exposed ($p = 0.026$) CRC animal models. No significant difference was observed among the three PD-1 blockade groups

in human CRC cells pretreated with the mitogen-activated protein kinase (MAPK) inhibitor PD98059 (APExBIO, 50 μmol/L), PI3K–AKT inhibitor wortmannin (APExBIO, 10 μmol/L), or STAT1 inhibitor Fludara (APExBIO, 50 μmol/L) by FCM. As shown in Fig. 5c, d, PD-L1 expression was significantly downregulated in different MSI status cell lines pretreated with Fludara. By contrast, there was no significant alteration in PD-L1 expression after treatment with PD98059 or wortmannin, which inhibited the MAPK and PI3K–AKT pathways, respectively.

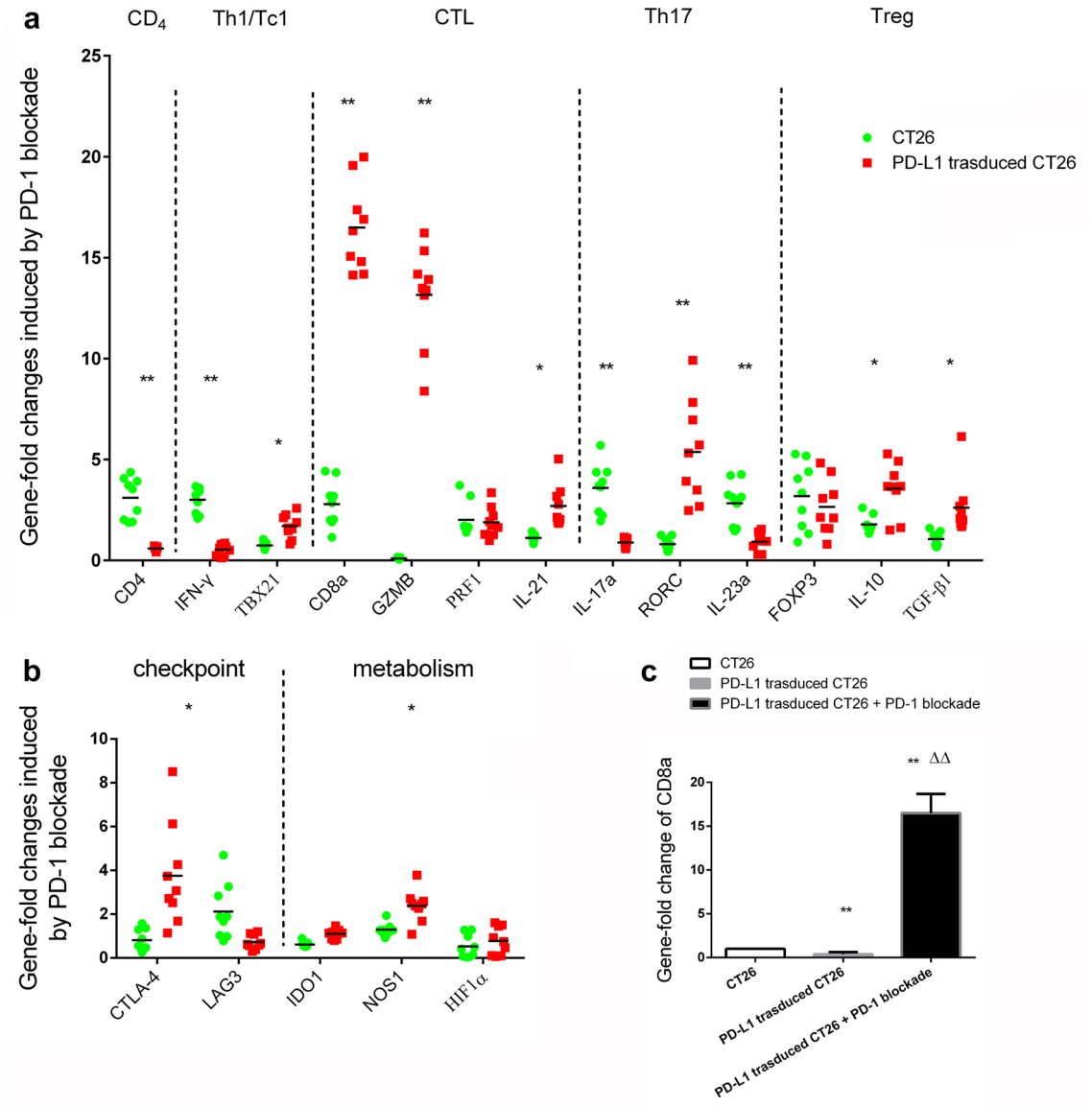

Fig. 4 Immune-related gene expression profiles were assessed using qPCR for selected genes. Sets of genes were defined by functional relevance. **a** CD_4, Th1/Tc1, CTL, Th17, and Treg; **b** immune checkpoint and metabolism. To analyze the different responses to PD-1 blockade in animal models with CT26 injection (the legend is "CT26", blue) or PD-L1 overexpressing CT26 injection (the legend is "PD-L1 transduced CT26", red), we calculated the fold change in gene expression using the $2^{-\Delta\Delta Ct}$ method. *Statistically significant differences, $p<0.05$; **$p<0.001$. **c** In this case, the fold change in CD8a was further analyzed, and the fold change in group 1 (CT26) was specified as 1. **$p<0.001$ vs. group 1; $^{\Delta\Delta}p<0.001$ vs. group 3 (PD-L1 transduced CT26)

Different JAK–STAT signaling molecules participated in low-dose IFNγ-induced PD-L1 expression in MSI-H and MSS colorectal cancer cell lines in vitro

We used a RT^2 Profiler PCR Array and measured the mRNA levels of 84 genes associated with the JAK–STAT signaling pathway. As shown in Supplementary Fig. 1, 19 genes demonstrated a greater than twofold change, and 2 genes were downregulated in cultured HCT116 cells compared with those in SW480 cells. As shown in Table 1, after treatment with 100 IU/mL IFNγ for 12 h, the most striking result was the strong upregulation of chemokine (C-X-C motif) ligand 9 (CXCL9) in HCT116 (68.53-fold) and SW480 cells (100.19-fold). As expected, STAT1, STAT4, IRF1 and IRF9 were mildly overexpressed with IFNγ interference in both cell lines. However, JAK2 (2.11-fold), as well as SATA2/3 (2.06-fold and 2.04-fold, respectively), was upregulated in SW480 cells only, and downregulation of JAK3 (2.87-fold) and STAT5A/5B (2.14-fold and 2.06-fold, respectively) was observed in HCT116 cells only after stimulation with a low

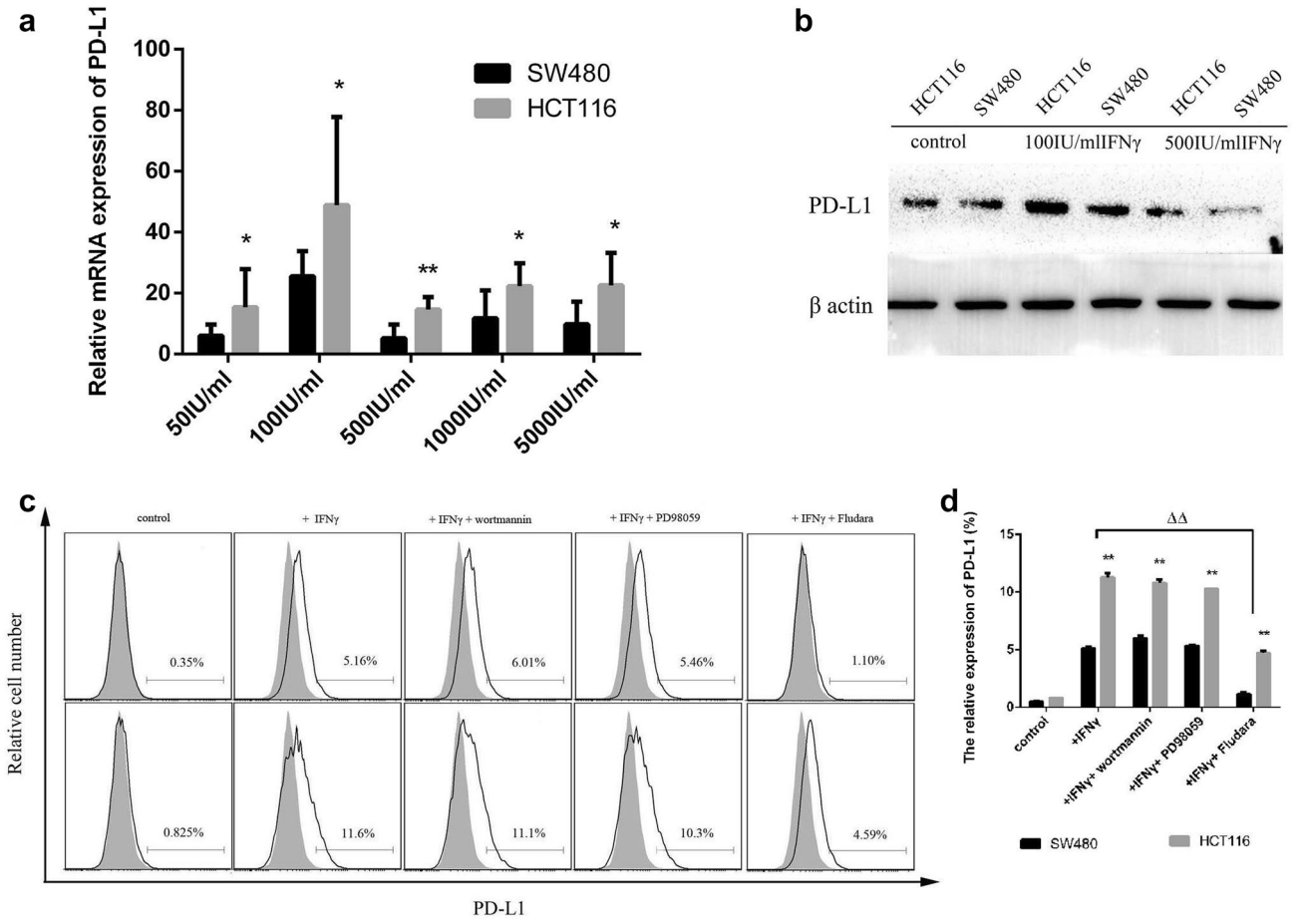

Fig. 5 Effects of IFNγ and kinase inhibitors on PD-L1 expression in the HCT116 and SW480 cell lines. **a** PD-L1 mRNA relative expression induced by different concentrations of IFNγ was measured by qPCR. **b** Expression levels of the PD-L1 protein stimulated with 100 IU/mL or 500 IU/mL IFNγ for 12 h. **c, d** PD-L1 expression was measured by flow cytometry in SW480 (the upper line) and HCT116 (the lower line) cell lines 12 h after treatment with 100 IU/mL IFNγ, with 1 μmol/L wortmannin, 50 μmol/L PD98059, or 50 μmol/L Fludara. DMSO was used as a vehicle and negative control (*$p < 0.05$, **$p < 0.001$ vs. SW480, $^{\Delta\Delta}p < 0.001$ *vs*. cells treated with IFNγ and DMSO)

level of IFNγ. SOCS1 demonstrated higher upregulation in SW480 cells after treatment with IFNγ than in HCT116 cells (5.84-fold vs. 3.95-fold).

Discussion

Based on data from clinical trials, the US FDA granted approval for use of pembrolizumab and nivolumab for treatment for adults with dMMR and MSI-H metastatic or progressive CRC. This approval changes the landscape of cancer immunotherapy but also raises some questions. The response to PD-1 blockade is not uniform across all MSI CRC patients. Furthermore, only 5–15% of CRCs display the MSI-H genotype, leaving the majority of patients with the MSS profile. If the mechanism of the heterogeneity of the response to anti-PD-1 therapy is elucidated, it could guide clinicians to identify potentially targetable factors and determine therapeutic strategies to enhance responsiveness to PD-1 blockade immunotherapy in most patients with CRC.

In this study, higher PD-L1 expression contributed to a higher tumor weight. Here, PD-L1 overexpression in CT26 cancer cells was also concomitant with decreased expression of CD8a genes and a lower apoptotic rate of tumor tissue cells. These results are partly in agreement with previous studies [23, 24] showing that overexpression of PD-L1 in vitro accelerated the proliferation and anti-apoptosis of cancer cells by facilitating cell cycle progression. Moreover, extrinsic IFNγ treatment induced extensive PD-L1 expression in neoplastic cells as well as in tumor-infiltrating lymphocytes. However, the challenge had no obvious effect on the rate of cell apoptosis in tumor-infiltrated tissues. The discrepancy probably demonstrates that PD-L1 expression induced by low-level IFNγ exposure in tumor tissues reflects the adaptive immune response, whereas PD-L1

Table 1 Gene fold changes associated with the JAK/STAT signal pathway after treatment of the SW480 and HCT116 cell lines with 100 IU/mL IFNγ for 12 h

SW480		HCT116	
Gene symbol	Fold regulation	Gene symbol	Fold regulation
A2M	4.2	A2M	2.33
CXCL9	100.19	CCND1	−2.06
IL4	−2.24	CEBPB	−2.45
IRF1	9	CXCL9	68.53
IRF9	8.95	EGFR	−2.03
ISG15	2.26	FCGR1A	6.38
JAK2	2.11	IL2RA	−6.82
OSM	−2.12	IL2RG	−3.02
SOCS1	5.84	INSR	−2.6
SOCS2	−2.79	IRF1	5.81
STAT1	21.83	IRF9	5.45
STAT2	2.06	ISG15	2.05
STAT3	2.04	JAK3	−2.87
STAT4	2.58	LRG1	−2.13
B2M	3.25	PDGFRA	−3.47
		PTPN11	−2.13
		SOCS1	3.95
		SOCS2	−2.7
		SRC	−2.05
		STAT1	14.92
		STAT4	10.49
		STAT5A	−2.14
		STAT5B	−2.06
		B2M	3.11

overexpression in CT26 cells represents the intrinsic anti-apoptotic mechanism. Specifically, PD-1 blockade immunotherapy significantly inhibited tumor growth in all CRC mice in this study. As in other studies [7–10], the enhanced number of $CD8^+$ cells and decreased neoplastic cells, in line with increased apoptotic cells in tumor-infiltrated tissues, were observed in this study. Importantly, we observed apoptotic neoplastic cells after anti-PD-1 immunotherapy. In a tumor microenvironment, neoplastic cells induced a T cell response, and consequently, activated T cells released IFNγ, which induced neoplastic cells expressing PD-L1. After binding to PD-1, PD-L1 delivered a suppressive signal to $CD8^+$ lymphocytes and induced exhaustion of the T cell immune response. PD-1 mAb treatment reinvigorated $CD8^+$ cells to maintain their effector function, eliminate neoplastic cells through GZMB, and secrete cytokines that recruit other immune cells to participate in the antitumor response. Interestingly, PD-1 blockade immunotherapy in those two high PD-L1 expression profiles results in a greater extent of tumor rejection, in line with the enhanced expression of CTL genes compared with that in CT26 cell-injected models treated with the same blockade. However, higher expression of PD-L1 did not influence the weight of terminal tumors harvested on day 30 in animal models administered PD-1 mAb therapy. All of these data suggest that PD-L1 may mainly be associated with anti-apoptosis of cells in the tumor microenvironment. However, treatment with PD-1 blockade significantly inhibited tumor growth, accompanied by an obviously enhanced CTL gene profile as well as a cell apoptosis phenomenon. Consistent with other studies [8–10], our experiment suggests that PD-1 blockade therapy plays a remarkable role in tumor rejection, possibly by infiltrating CTLs, which promote neoplastic cell apoptosis in the CRC microenvironment.

Alternatively, we also observed that compared with the SW480 cell line, the HCT116 cell line, which lacks the MLH1 protein and usually represents MSI-H CRC, displayed higher relative mRNA expression of PD-L1 in vitro after stimulation by a different concentration of IFNγ. This result is also consistent with most clinical investigations [2, 11, 12] showing that MSI-H patients have a significantly higher rate of positive PD-L1 expression. Although a recent study [20] was compelling regarding whether the higher density of PD-L1 was expressed in tumor cells or in tumor-infiltrating myeloid cells in the stroma of CRC, we demonstrated here that PD-L1 was extensively expressed on neoplastic cells as well as $CD8^+$ lymphocytes in tumors harvested from mice with CRC. All of the aforementioned results suggest that higher PD-L1 expression in CRC cells is partly associated with PD-1 blockade therapy. Most importantly, the correlation that we observed in this experiment is probably due to internal genetic or epigenetic modifications that occur in CRC cells exposed to IFNγ, which are mainly produced by CTLs in the tumor microenvironment. Experimentally, higher expression of PD-L1 in CT26 cells acted like a high-level molecular shield, resulting in anti-apoptosis of cells, decreased numbers of $CD8^+$ lymphocytes and decreased mRNA expression of CTL. With PD-1 mAb therapy, the positive response that we observed between PD-L1 overexpression and increased CTLs in CT26 subcutaneous tumors suggests a fine-tuned regulation of in situ inflammatory recruitment, but whether the CTL profile is the cause or consequence of immune infiltration remains unclear.

IFNγ is considered to have a dual effect on anti-tumor immunity. A number of studies have pointed to a similar conclusion; IFNγ plays a central role in the recognition and elimination of transformed cells because of its cytostatic, pro-apoptotic and immune-provoking effects [15]. We also observed that cultured SW480 and HCT116 cells partly became round and nonadherent after treatment with 5000 IU/mL IFNγ. Nevertheless, stimulation with 100 IU/mL IFNγ led to significant enhancement of PD-L1 expression, especially in HCT116 cells. In an in vivo setting, low-level IFNγ challenge also decreased the number of $CD8^+$

cells in the tumor microenvironment. Thus, we conclude that a large dose of IFNγ leads to anti-tumor immunity, whereas low-level IFNγ most likely has an immune modulatory function. However, we should consider that large doses of IFNγ also induced the expression of PD-L1 in CRC cells, especially in the MSI-H cell line. Therefore, researchers should be cautious when using IFNγ as a therapeutic agent for cancer treatment.

Moreover, we observed that the upregulation of PD-L1 induced by IFNγ was mainly associated with activation of the JAK–STAT but not the MAPK and PI3K–AKT pathways in CRC cell lines in vitro. However, according to previous studies, PD-L1 expression stimulated by IFNγ is controlled by the MAPK or PI3K–AKT pathways [16, 17]. These results suggest that PD-L1 regulation by IFNγ might be mediated through different pathways depending on the cell type. PD-L1 expression in CRC cells was mainly triggered by previously described JAK–STAT signals, but in some instances, intrinsic cell alteration also contributed to extrinsic PD-L1 induction. Partial differential molecular mechanisms associated with the JAK–STAT signaling pathway might contribute to such hyperresponsiveness to low doses of IFNγ exposure in the MSI-H cell line. Our data demonstrated that extrinsic IFNγ-induced PD-L1 expression was mainly JAK2–SATA2/3 dependent in SW480 cells but JAK3–STAT5A/5B related in HCT116 cells. Notably, SOCS1, a negative feedback regulator of IFNγ/STAT signaling that inhibits JAK tyrosine kinase activity [25], displayed higher upregulation in SW480 cells treated with IFNγ than in HCT116 cells. However, we also observed downregulation of IL-2RA (6.82-fold) and EGFR (2.03-fold) only in HCT116 cells stimulated with IFNγ. Recently, one study [26] suggested that loss of IFNγ pathway genes in tumor cells is a mechanism of resistance to anti-CTLA-4 therapy. Therefore, HCT116, a MSI-H cell line, exhibits selective hyperresponsiveness to the IFNγ pathway, which contributes to the increased PD-L1 expression and may be a mechanism of response to anti-PD-1 therapy in CRC.

In conclusion, our study demonstrated that PD-L1 expression in CRC induced a tumor-shielding response. Combined with PD-1 blockade immunotherapy, PD-L1 expression probably caused the higher extent of tumor rejection, in line with the enhanced expression of CTL genes. PD-L1 expression was significantly upregulated by low-dose IFNγ treatment, and the MSI-H cell line might exhibit hyperresponsiveness to IFNγ exposure. Furthermore, intrinsic PD-L1 expression in cooperation with extrinsic IFNγ exposure likely participated in the response mechanism to anti-PD-1 therapy, mainly through the CTL profile in the tumor microenvironment. Although this result provides novel insights into the mechanism by which anti-PD-1 therapy focuses on hyperresponsiveness to IFNγ, questions remain with respect to detailed alterations in PD-L1 in neoplastic cells that could critically affect PD-1 blockade responses in CRCs. Further work is needed to elucidate the complicated mechanisms.

Acknowledgements We would like to thank Xiaojin Li (Central laboratory, the second hospital of Yunnan Province) for his technical assistance in flow cytometry.

Author contributions Conceived and designed the experiments: WY and JD. Performed the experiments: WY, CT, XS, HJ and HH. Analyzed the data: WY and JD. Contributed reagents/animals: DD, HJ and RN. Wrote the paper: WY and JD.

Funding This study was partially supported by the Association Foundation Program of Yunnan Provincial Science and Technology Department and Kunming Medical University (Grant number: 2017FE468(-228)), by the Foundation of Yunnan Medical Science and Technology (Grant number: 2016NS124), and by the National Natural Science Foundation of China (Grant number: 81660472).

Compliance with ethical standards

Conflict of interest The authors declare no conflicts of interest.

Ethical approval and ethical standards The animal study was approved by the Animal Experimental Ethical Committee of Kunming Medical University (date of approval: June 2017). The experimental mice used in this study were obtained from the Laboratory Animal Center of Kunming Medical University. All experimental procedures were conducted according to the protocols approved by the National Institute of Health's Guidelines for the Care and Use of Laboratory Animals. This article does not contain any studies with human participants performed by any of the authors.

Cell line authentication Human CRC cell lines HCT116 and SW480 were obtained from the Institute of Zoology, Chinese Academy of Sciences (Kunming, China), and rat CRC CT26 cells were purchased from the Cell Bank of the Chinese Academy of Sciences (Shanghai, China). Cell Bank, Type Culture Collection, Chinese Academy of Sciences (CBTCCCAS) can provide the Certificate of STR Analysis.

References

1. Westdorp H, Fennemann FL, Weren RD et al (2016) Opportunities for immunotherapy in microsatellite instable colorectal cancer. Cancer Immunol Immunother 65:1249–1259
2. Bupathi M, Wu C (2016) Biomarkers for immune therapy in colorectal cancer: mismatch-repair deficiency and others. J Gastrointest Oncol 7:713–720
3. Marisa L, Svrcek M, Collura A et al (2018) The balance between cytotoxic T-cell lymphocytes and immune checkpoint expression in the prognosis of colon tumors. J Natl Cancer Inst. https://doi.org/10.1093/jnci/djx136
4. Miguchi M, Hinoi T, Shimomura M et al (2016) Gasdermin C is upregulated by inactivation of transforming growth factor β receptor type II in the presence of mutated Apc, promoting colorectal cancer proliferation. PLoS One 11:e0166422
5. Ogawa M, Watanabe M, Hasegawa T et al (2017) Expression of CXCR-4 and IDO in human colorectal cancer: an immunohistochemical approach. Mol Clin Oncol 6:701–704

6. Johdi NA, Ait-Tahar K, Sagap I et al (2017) Molecular signatures of human regulatory T cells in colorectal cancer and polyps. Front Immunol 8:620
7. Kim ST, Klempner SJ, Park SH et al (2017) Correlating programmed death ligand 1 (PD-L1) expression, mismatch repair deficiency, and outcomes across tumor types: implications for immunotherapy. Oncotarget 8:77415–77423
8. Javed A, Arguello D, Johnston C et al (2017) PD-L1 expression in tumor metastasis is different between uveal melanoma and cutaneous melanoma. Immunotherapy 9:1323–1330
9. Oya Y, Yoshida T, Kuroda H et al (2017) Predictive clinical parameters for the response of nivolumab in pretreated advanced non-small-cell lung cancer. Oncotarget 8:103117–103128
10. Bedke J, Stühler V, Stenzl A et al (2018) Immunotherapy for kidney cancer: status quo and the future. Curr Opin Urol 28:8–14
11. Lee KS, Kwak Y, Ahn S et al (2017) Prognostic implication of CD274 (PD-L1) protein expression in tumor-infiltrating immune cells for microsatellite unstable and stable colorectal cancer. Cancer Immunol Immunother 66:927–939
12. Toh JWT, de Souza P, Lim SH et al (2016) The potential value of immunotherapy in colorectal cancers: review of the evidence for programmed death-1 inhibitor therapy. Clin Colorectal Cancer 15:285–229
13. Korehisa S, Oki E, Iimori M et al (2018) Clinical significance of programmed cell death-ligand 1 expression and the immune microenvironment at the invasive front of colorectal cancers with high microsatellite instability. Int J Cancer 142:822–832
14. Ritprajak P, Azuma M (2015) Intrinsic and extrinsic control of expression of the immunoregulatory molecule PD-L1 in epithelial cells and squamous cell carcinoma. Oral Oncol 51:221–228
15. Kursunel MA, Esendagli G (2016) The untold story of IFN-γ in cancer biology. Cytokine Growth Factor Rev 31:73–81
16. Mimura K, Teh JL, Okayama H et al (2017) PD-L1 expression is mainly regulated by interferon gamma associated with JAK–STAT pathway in gastric cancer. Cancer Sci 109:43–53
17. Zhang X, Zeng Y, Qu Q et al (2017) PD-L1 induced by IFN-γ from tumor-associated macrophages via the JAK/STAT3 and PI3K/AKT signaling pathways promoted progression of lung cancer. Int J Clin Oncol 22:1026–1033
18. Kuttke M, Sahin E, Pisoni J et al (2016) Myeloid PTEN deficiency impairs tumor-immune surveillance via immune-checkpoint inhibition. Oncoimmunology 5:e1164918
19. Dong ZY, Zhang JT, Liu SY et al (2017) EGFR mutation correlates with uninflamed phenotype and weak immunogenicity, causing impaired response to PD-1 blockade in non-small cell lung cancer. Oncoimmunology 6:e1356145
20. Llosa NJ, Cruise M, Tam A et al (2015) The vigorous immune microenvironment of microsatellite instable colon cancer is balanced by multiple counter-inhibitory checkpoints. Cancer Discov 5:43–51
21. Wang L, Liu Z, Fisher KW et al (2018) Prognostic value of programmed death ligand 1, p53, and Ki-67 in patients with advanced-stage colorectal cancer. Hum Pathol 71:20–29
22. Xu JX, Xiong W, Zeng Z et al (2017) Effect of ART1 on the proliferation and migration of mouse colon carcinoma CT26 cells in vivo. Mol Med Rep 15:1222–1228
23. Okita R, Maeda A, Shimizu K et al (2017) PD-L1 overexpression is partially regulated by EGFR/HER2 signaling and associated with poor prognosis in patients with non-small-cell lung cancer. Cancer Immunol Immunother 66:865–876
24. Tao LH, Zhou XR, Li FC et al (2017) A polymorphism in the promoter region of PD-L1 serves as a binding-site for SP1 and is associated with PD-L1 overexpression and increased occurrence of gastric cancer. Cancer Immunol Immunother 66:309–318
25. Berzaghi R, Maia VS, Pereira FV et al (2017) SOCS1 favors the epithelial-mesenchymal transition in melanoma, promotes tumor progression and prevents antitumor immunity by PD-L1 expression. Sci Rep 7:40585
26. Gao J, Shi LZ, Zhao H et al (2016) Loss of IFN-γ pathway genes in tumor cells as a mechanism of resistance to anti-CTLA-4 therapy. Cell 167:397–404